Heat-Accumulation Stoves: Numerical Simulations of Two Twisted Conduit Configurations

P. Scotton[*1], D. Rossi[1], M. Barberi[2], S. De Toni[2]
[1]Geosciences Department of Padova University, [2]Barberi Stufe LTD
*G. Gradenigo Str. N° 6, 35131 Padova (Italy); paolo.scotton@unipd.it

Abstract: An important part of the society considers an increased share of renewable energies as an integral part of a strategy towards a sustainable future. As far as heat supply is concerned, this can be achieved using solar thermal collectors, borehole heat exchangers or trough the combustion of biomass. This article shows two applications of two configurations of twisted conduit inside the external coating of the heat accumulation stoves. The hydrodynamic flow is described by the k-ϵ model, the buoyancy is taken into account, the heat transmission is treated into its three components: conductive, convective and radiative. The numerical results are compared with experimental measurements performed in the same configurations. The experimental data were also used to determine the initial and boundary conditions of the numerical calculations. This research follows a multidisciplinary approach (numerical and physical modelling) to describe the hydrodynamic flow and the heat exchanges between flue gas and the refractory material.

Keywords: Non-isothermal Flow, Turbulent Flow, Heat Transfer, Dynamics of Flue Gases, Finite Element Simulations

1. Introduction

A traditional stove in the Alpine regions is the heat-accumulation stove, made of refractory blocks and a covering of ceramic tiles. This particular kind of stoves consist of a combustion chamber, where woody material is burned, followed by a twisted conduit where the high temperature flue gas flows, giving off heat to the refractory. The internal geometric arrangement of the conduit, with rapid sequence of curves, as well as its shape and roughness, influence the hydrodynamics of the flue gas. The thermodynamic properties of the refractory material, its mass and its geometric arrangement, are other main parameters of the stove's functionality. Sometimes a coating, made of panels of refractory material, is constructed around the twisted conduit in order to create an air cavity, where the thermal energy is redistributed by natural convection and radiation. This article follows two papers presented in previous Comsol conferences (Stuttgart 2011 [1], Boston 2012 [2]) and shows two applications in two configurations of the twisted conduit, in the absence of the external coating. In the first case (configuration F8) the conduit is developed in two dimensions, on a vertical plane, in the second case (configuration F9) is developed in three dimensions (Figure 1). In the present paper, the numerical results, obtained reproducing the two mentioned configurations under unsteady flow regime, are showed.

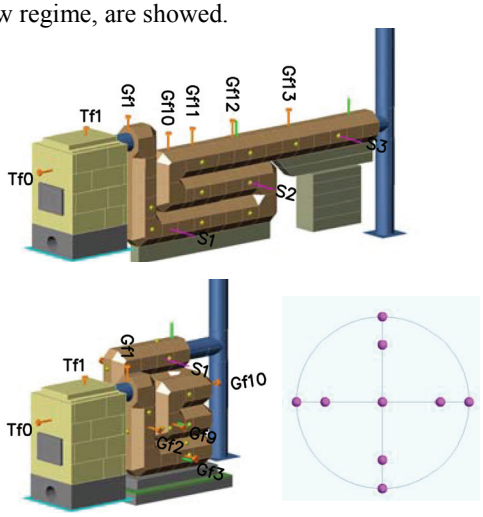

Figure 1 Above, the configuration of a twisted conduit developed on a vertical plane (F8); below, the configuration with vertical and horizontal curves (F9); below on the right, the scheme of an instrumented section showing the position of nine thermocouples.

2. Experimental Apparatus

From the physical experiments the flue gas temperatures, the pressure drop along the conduit and the gases velocity at some sections have been obtained.

The experimental apparatus is composed of a stove (61 cm × 68 cm × 112 cm), connected to the refractory conduit by means of a short steel pipe (length equal to 30 cm). In the first study case, the refractory conduit performs a sequence

of vertical curves and its length is 664 cm; in the second study case the curves are both horizontal and vertical and the length of the conduit is 638 cm. In both cases the internal diameter is 18 cm and the end of the conduit is connected to the chimney through a T connection.

The temperature measurements were made both in the center of the conduit by means of K thermocouples and on the outer surface of the refractory conduit by means of T thermocouples. In order to investigate the themperature distribution inside the cross sections, three instrumented sections with nine thermocouples were made. The nine sensors were placed in a cross-shaped distribution, as showed in Figure 1. The implementation of the thermo-fluid-dynamics is a challenging numerical problem due to the high temperatures of the flue gas. The temperatures at the inlet of the refractory conduit, are showed in the upper chart of Figure 2.

The combustion air was supplied through a steel pipe where the velocity and the temperature were taken by means of a hot wire anemometer and a thermocouple. The estimation of the mass discharge of the flue gas, starting from the mass discharge of combustion air, was made in agreement with the EN 15544. Figure 2 shows the mass discharge of flue gas of the two configurations.

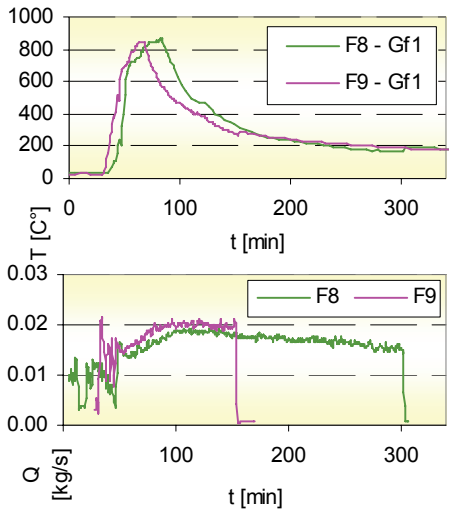

Figure 2 Above, the temperatures at the sensores Gf1 (Figure 1); below, the mass discharge of flue gas evaluated starting from the mass discharge of combustion air using the EN 15544 regulations.

3. Governing Equations

3.1 Fluid dynamics

The Navier – Stokes equations describe the motion of viscous fluids. For a single-phase flow they are composed by the continuity equation (Eq 1), the momentum equation (Eq 2),where the viscous stress tensor is given by the equation 3.

$$\frac{\partial \rho}{\partial t} + \nabla \cdot \left(\rho \vec{u}\right) = 0 \qquad \textbf{Eq 1}$$

$$\rho \frac{\partial \vec{u}}{\partial t} + \rho\, \vec{u} \cdot \nabla \vec{u} = -\nabla p + \nabla \cdot \tau + F \qquad \textbf{Eq 2}$$

$$\tau = \mu\left(\nabla \vec{u} + \nabla \vec{u}\Big|^{T}\right) - \frac{2}{3}\mu\left(\nabla \cdot \vec{u}\right)\overline{\overline{\mathrm{I}}} \qquad \textbf{Eq 3}$$

For turbulent flows the Navier – Stokes equations are simplified, through the average over the time, in the Reynolds – Averaged Navier Stokes (RANS) equations [3] [4]. In the term F, to the right hand of equation 2, are present also the buoyancy forces, responsible for the flow stratification and for the natural draught of the stove. The density is, however, a variable of the problem and depends on the temperature. Therefore, the buoyancy forces can be introduced in the momentum equations through the first Boussinesq approximation:

$$F = -\left(\rho - \rho_R\right) g \qquad \textbf{Eq 4}$$

3.2 Heat transport

The heat transfer in a physical system is provided by conduction, convection and radiation. For conduction in a multidimensional isotropic system, the Fourier law can be rewritten in the form [5] [7]:

$$q = -k \nabla T \qquad \textbf{Eq 5}$$

The convection heat transfer, which occurs between a wall at temperature T_W and the surrounding atmosphere at undisturbed temperature T_∞, can be represented by the equation:

$$q = h\left(T_W - T_\infty\right) \qquad \textbf{Eq 6}$$

where $h = Nu \cdot k / d$.

In the study of the heat transfer by radiation, in the cases where heat is supplied to the physical system by combustion of any fuel type, the flue gas has to be considered as a participant medium. It is composed of a fraction of molecular gas and a part of particulate matter. Its interaction with the radiative intensity travelling

in a given direction ($\mathrm{I}(\Omega_i)$) occurs through absorption, emission and scattering [6].

The radiation absorption of the particulate matter has been observed to be proportional to the magnitude of the incident energy as well as the distance the beam travels (s) through the medium:

$$\frac{d\mathrm{I}_{abs}}{ds} = -\kappa \mathrm{I}(\Omega; s) \quad \textbf{Eq 7}$$

At the given temperature T, the rate of emission from a volume element will be equivalent to a fraction of emission intensity of the black body:

$$\frac{d\mathrm{I}_{em}}{ds} = \kappa \mathrm{I}_b(T) \quad \textbf{Eq 8}$$

The scattering can be distinguished in out–scattering and in-scattering. The out–scattering considers the part of incoming intensity that is deviated from the considered direction of propagation. The out–scattering intensity appears, therefore, as augmentation energy (in-scattering) along another direction.

$$\frac{d\mathrm{I}_{out-sc}}{ds} = -\sigma_s \mathrm{I}(\Omega; s) \quad \textbf{Eq 9}$$

The in-scattering has contributions from all directions and, therefore, must be calculated by integration over all solid angles Ω_i:

$$\frac{d\mathrm{I}_{in-sc}}{ds} = -\sigma_s/(4\pi)\int_{4\pi} \mathrm{I}(\Omega_i)\phi(\Omega_i;\Omega)d\Omega_i \quad \textbf{Eq 10}$$

Considering the two terms of attenuation, absorption and out-scattering, leads to define the extinction coefficient through the path s:

$$\frac{d\mathrm{I}_{extinction}}{ds} = -\beta \mathrm{I}(\Omega; s) \quad \textbf{Eq 11}$$

where $\beta = \kappa + \sigma_s$ is the extinction coefficient.

The equation of heat transfer by radiation (Radiation Transfer Equation – RTE), in the direction of solid angle ($\Omega \cdot \nabla \mathrm{I}(\Omega)$ reads [6] [7]:

$$\kappa \mathrm{I}_b(T) - \beta \mathrm{I}(\Omega; s) - \frac{\sigma_s}{4\pi}\int_{4\pi} \mathrm{I}(\Omega_i)\phi(\Omega_i;\Omega)d\Omega_i \quad \textbf{Eq 12}$$

Another component of heat transfer by radiation occurs between the outer surface, at temperature T_W, and the surrounding ambient at undisturbed temperature T_∞. This component of heat exchange can be written as:

$$q = \varepsilon\sigma\left(T_\infty^4 - T_W^4\right) \quad \textbf{Eq 13}$$

4. Numerical Model

The numerical models were implemented from the first short steel pipe, necessary to connect the stove to the refractory conduit, to the cross section located on the chimney, 2.7 m above the floor. In both configurations, it was not possible to take advantage of the symmetry due to the non symmetry of the radiation in participating media. The geometries were realised in CAD enviroment, exported in *.sat format and imported in the COMSOL environment.

The physical phenomena evaluated are: the fluid dynamics with the buoyancy forces and the heat transfer with the radiation in the participating media.

The physical phenomena that occur in an accumulation stove, once the activation energy in the combustion chamber has been provided, continue, initially increasing temperature and velocity of flue gases and then decreasing the two variables until the end of the reaction. This causes a continuous variation in the motion conditions at the inlet of refractory conduit. Due to the Reynolds number that increases in time (Figure 3), the k-ε model has been used. The coupled physics, the heat transfer, has been treated into its three components: conductive, convective and radiative. This last is treated with the Discrete-Ordinate Approximation method S2 for what concerns the size of the solid angle of radiation [6] [7]. The values of absorption and scattering used are respectively equal to 0.8307 [1/m] and 0.0 [1/m].

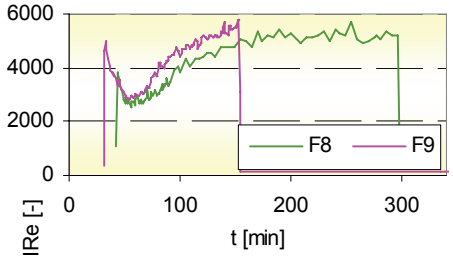

Figure 3 Reynolds number evaluated at the inlet face from the measured data.

4.1 Boundary conditions

The boundary conditions for the unsteady problem are the pressure at the final cross section and mass discharge (calculated using the literature equations reported in EN 15544 [8]) at

the initial section. In these numerical models the buoyancy forces have been considered using the first Boussinesq approximation (Eq 4).

Similarly for the heat transfer an outflow condition at the final cross section and a time-variable temperature on the first cross section have been imposed. In addition, on the outer surface of refractory conduit, a boundary condition of convective cooling (Eq 6) was used together with a boundary condition for the radiation from surface to the ambient (Eq 13).

4.2 Mesh and solvers

In our previous applications, that took into account the radiation in partecipating media, we obtained the best results using a tetrahedral mesh without a boundary layer. Although this causes a bad rappresentation of flow dynamics and heat transfer near the wall of the refractory conduit, a tetrahedral mesh was used (Figure 4). In the first configuration 36.274 were the total number of elements and 771.075 were the degrees of freedom, whereas in the second configuration 84.598 were the total number of elements and 1.050.000 were the degrees of freedom.

For reasons of stability, for both models a direct solver has been used. The characteristics of the workstation are: two Intel® Xeon® CPU X5550, 2.67 GHz (eight processors) and 24GB ram with a 64 bit software.

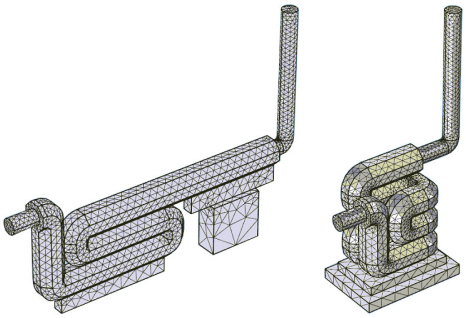

Figure 4 The meshes used for the two configurations: left F8, right F9.

5. Results and Discussion

5.1 Mass and Energy Balance

The equation of the mass balance reads:

$$Qm_{inp} - Qm_{out} = \left.\frac{dm}{dt}\right|_V \qquad \textbf{Eq 14}$$

where the first two terms are the in-mass discharge and the out-mass discharge, and the term on the right represents the mass variation in the time in the volume V. The mass balance was satisfactory for all the configurations, until the models were stable. Figure 5 shows the mass balance for the configuration F8; similar results has been obtained for F9 configuration.

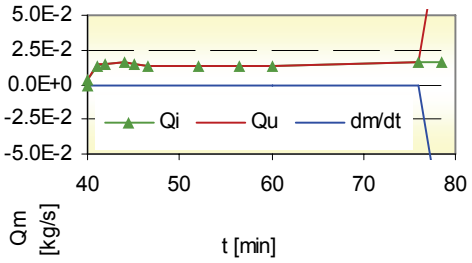

Figure 5 Mass balance for the configuration F8.

For open systems the energy balance equation reads:

$$\dot{E}_{inp} - \dot{E}_{out} - \dot{q} = \left.\frac{dE}{dt}\right|_V \qquad \textbf{Eq 15}$$

where the first two terms are the variation in time of the input and the output energy, the third term is the variation of heat exchange through the internal walls of the refractory conduit. The term on the right of the equation is the energy change in time in the volume V. For all the configurations the energy balance was not satisfactory. The sum of all terms of equation 15 should be near to zero; instead of zero, value of the order of thousand Watt has been obtained with errors of about 15% – 30% of the incoming energy. Figure 6 shows the energy balance for the configuration F8; similar results has been obtained for F9 configuration.

These errors are probably due to the rough discretization of the fluid domain, and in particular to the absence of sufficiently small mesh elements near the internal wall of the refractory conduit.

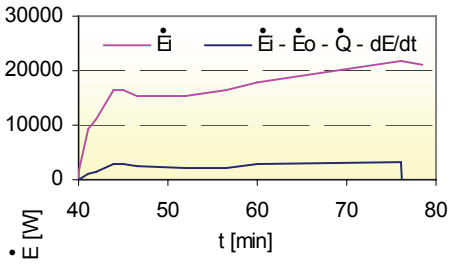

Figure 6 Energy balance for the configuration F8.

5.2 Mean Velocity Pressure and Temperature

In this section the velocities, temperatures and pressures, along the conduit are shown. The numerical results are averaged on every cross section. The measures of temperature and pressure were made at the center of the conduit.

A particularity is that the mean velocities, calculated with the numerical models, are not very different between the two configurations and the greatest differences are approximatively at the half of the path. The maximum velocity is about 2.25 m/s at the beginning of the conduit and the minimum velocity is about 1.15 m/s at its end (Figure 7 – A).

A similar discussion can be made for the temperatures of flue gas. Figure 7 – B shows with a solid line the calculated temperature with numerical model and with a dotted line that measured at the center of the conduit. As can be seen the decreasing trend of the temperature measured on the physical model follows the same behaviour, starting with 800 degrees at the begining of the conduit and reaching 180 degrees at its end. The simulations are not able to reproduce the temperature decrease with errors of the order to 200 degrees. Also in this case, the size of the error is likely ascribable to the absence of sufficiently small mesh elements near the internal wall of refractory conduit.

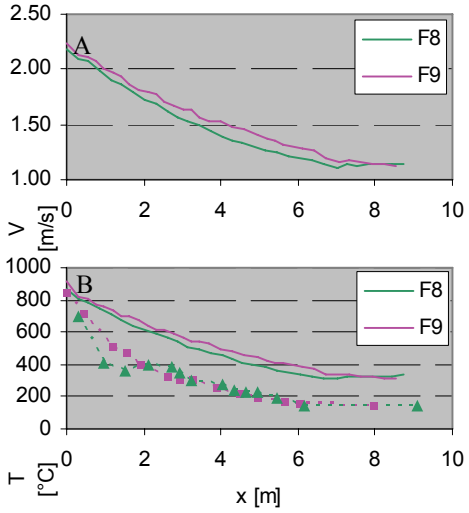

Figure 7 Above, calculated averaged velocities; below, measured temperature on physical model (dotted line) and calculated temperature (solid line), at the instant of maximum temperature of the flue gas at the inflow section.

Figure 8 shows with a dotted line the measured pressure at the center of the conduit and with a continuos line the calculated one. The measured pressure do not shows significant variations along the conduit with a maximum difference of about 5 Pa. It is visible, mainly in the F9 configuration, an initial pressure drop until the lower section of the pipe, then an increase of pressure that moves the pressure towards the atmospheric pressure. The calculated values of pressure show clearly the vertical steps of the twisted conduit. The horizontal lengths of the pipe in the F8 configuration does not have horizontal curves, whereas in the F9 configuration there are two horizontal curves. Due to this difference in the F9 configuration is more visible a pressure decrease along the horizontal sections of the conduit.

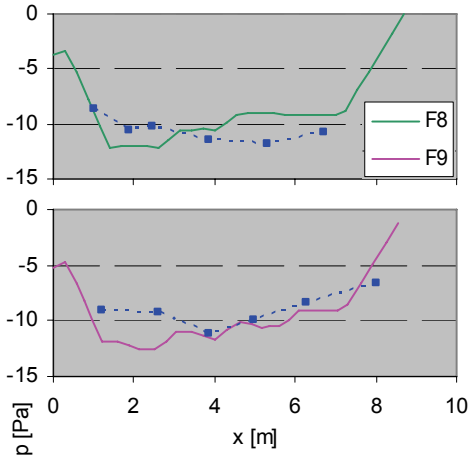

Figure 8 Measured (dotted line) and calculated (solid line) pressure: above, values for the F8 configuration; below, values for that F9.

5.3 Temperature on cross-section

This section presents a comparison between the measured and the calculated temperatures in some significant points of the conduit. As noted before, the calculated temperatures with the numerical model are greater than those measured on physical model.

Figure 9 shows the temperature values in the three instrumented cross-sections (Figure 1) of F8 configuration. In each section, the thermocouples have registered greater differences than those calculated by means of the numerical simulation. This differences are

reduced proportionally with the decrease of the mean temperature of the section.

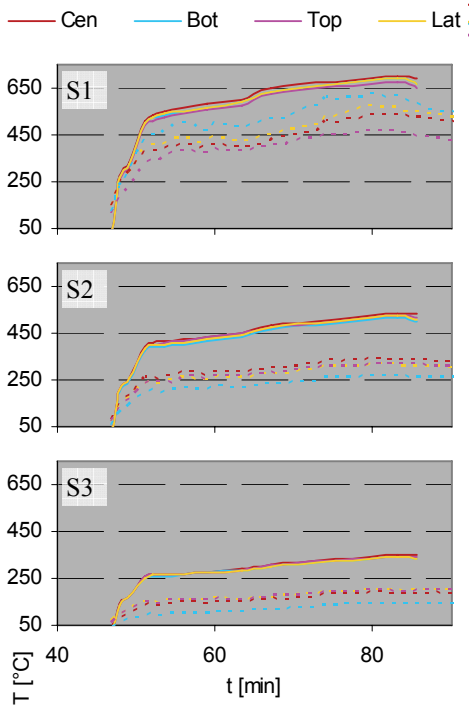

Figure 9 Measured (dl) and calculated (sl) temperatures in the three instrumented sections (Figure 1) present in the F8 configuration.

6. Conclusions

The present physical phenomenon has been faced solving the equations of thermo-fluid dynamics, considering the thermal radiation both internal and external to the pipe and the effects of buoyancy.

The equation of mass balance is correctly described until numerical intability occurs. The energy balance shows errors of the order of 10%, 15% of energy entering the system, until numerical intability occurs.

The numerical values of pressure don't differ significantly from the measured ones, taking also into account the experimental difficulties.

The numerical values of the velocity along the pipe, range from 2 m/s to 1m/s, consistently with the values assumed by the temperature.

The averaged temperature along the section is much higher than the measured temperature at the center of the section. The measured temperature variations along a section are much higher than the calculated ones. The temperature variations across the section, both numerical and experimental, decrease increasing the distance from the inflow section, namely decreasing the average temperature of the section.

In general, the numerical results are strongly dependent on the choice of the calculation mesh. The use of a boundary layer can lead to numerical instability.

Refining the mesh, higher precision is observed in the energy balance equation. In the presented problem, calculation times are not compatible, even with medium-high computing power, with the reduction of the error below a few percentage points.

Consequently the research is now moving towards a simplification of the numerical problem by searching a non coupled solution of the hydrodynamic and thermo-dynamic problem, suggested by the properties of the single physics.

7. References

1 Scotton P., Rossi D., Study of Gas Dynamics in the Heat-accumulation Stoves, *Comsol Conference 2011*, **Stuttgart Proceedings**, ISBN 978-0-9839688-0-1 (2011)

2 Scotton P. Rossi D., Barberi M., De Toni S., Thermo-Fluid Dynamics of Flue Gas in Heat Accumulation Stoves: Study Cases, *Comsol Conference 2012*, **Boston Proceedings**, ISBN 978-0-9839688-8-7 (2012)

3 Garde R. J., Turbulent Flow, **New Age International** (2010);

4 Comsol Multiphysics, CFD Module User's Guid;

5 Faghri A., Zhang Y., Howel J., Advanced Heat and Mass Transfer, **Global Digital Press**, Columbia, USA (2010);

6 Modest M. F., Radiative Heat Transfer, **McGraw Hill**, (1983);

7 Comsol Multiphysics, Heat Transfer Module User's Guid;

8 EN–15544, One of kachelgrundöfen putzgrundöfen (tiled mortared stoves) – calculation method;

8. Acknowledgements

The research has been financed by the Trentino (Italy) Provincial law n. 6, 1999, call 2008 - project: "La stufa ad accumulo-Innovazione nella tradizione" of the Barberi Ltd.

10. Symbols

d	diameter	[m]
h	convective coefficient	[W/(m^2 K)]
k	thermal conductivity	[W/(m K)]
κ	absorption coefficient	[1/m]
$\bar{\bar{\mathrm{I}}}$	identity matrix	[–]
I	radiative intensity	[–]
I_b	black body radiative intensity	[–]
μ	dynamic viscosity	[Pa]
Nu	Nusselt number	[–]
Ω_i	solid angle in i direction	[sr]
p	Pressure	[Pa]
q	heat flux	[W/m^2]
ρ	density	[kg/m^3]
ρ_R	reference density	[kg/m^3]
s	beam travel distance	[m]
σ_s	scattering coefficient	[1/m]
t	time	[s]
T	temperature	[°C]
T_W	wall temperature	[°C]
T_∞	undisturbed temperature	[°C]
T_R	reference temperature	[°C]
τ	viscous stress tensor	[Pa]
$\vec{u}$	velocity vector	[m/s]
dl	dotted line	
sl	solid line	